2017 WJTA-IMCA Conference and Expo
October 25-27, 2017 • New Orleans, Louisiana

Paper

NUMERICAL ANALYSIS OF THE THREE-MATERIAL DOWNHOLE FLOW FIELD IN HYDROTHERMAL JET DRILLING

Xianzhi Song, Zehao Lyu, Haizhu Wang, Gensheng Li

China University of Petroleum, Beijing

Beijing, China

ABSTRACT

Combined with high pressure water jet and thermal spallation drilling methods, hydrothermal jet drilling technology is proposed, which is expected to be suitable for deep hard formations and exploitation of geothermal energy. In this paper, compressible fluid and drilling cuttings are considered and the downhole flow field of the lateral cooling configuration is investigated. Distributions bottomhole temperature and pressure are analyzed. Influences of the jet temperature, cooling water velocity, volume fraction of carbon dioxide and type of cuttings on the flow field are discussed. Results indicate that there are two vortexes in the bottomhole space with the maximum carbon dioxide volume fraction. At 0.002 s, the hydrothermal jet reaches the well bottom. The volume fraction of carbon dioxide is 10% in most of the downhole space. During the drilling process, it may be better to keep the jet temperature close to the pseudo-critical temperature. The increase of cooling water velocity has no obvious effect on the carrying of drill cuttings. The addition of water can slightly enhance the bottomhole pressure. The maximum temperature decreases as the increase of rock density. The clean efficiency for low density rocks is higher.

1 INTRODUCTION

Hydrothermal jet drilling is an alternative drilling technology, which has the potential to be applied for petroleum and geothermal energy in deep hard formations [1, 2]. This technique intends to combines the advantages of thermal spallation effect [3, 4] and high pressure water jet [5, 6] to break the bottom rock. The coiled tubing is used for continuous penetration. Fuel, oxidizer and cooling water are injected through respective channels down coiled tubing to the downhole combustion chamber (**Figure 1**). The chemical reaction between the fuel and the oxidizer in the chamber is initiated by an electric spark. Thus, the reaction products, which are water and carbon dioxide, are ejected from the nozzle in the bottomhole assembly to impinge on the rock. Meanwhile, cooling water flows out from the lateral outlet of coiled tubing and returns to the surface through the annulus. This can cool the wellbore and coiled tubing simultaneously, and avoid the thermal destruction on the borehole wall by the high temperature fluids. Moreover, the circulation of cooling water can increase the cuttings transport efficiency. Thermal insulation is applied around coiled tubing to keep the cooling water from influences of reservoir temperature or combustion.

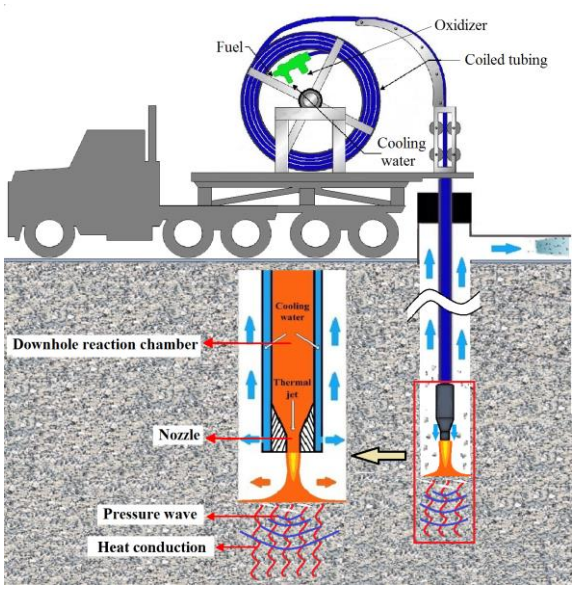

Figure 1. Coiled-tubing-deployed hydrothermal jet drilling concept

In 2016, Song et al. investigated the downhole flow field with multi-orifice nozzle and the thermo-physical interaction between wellbore fluid and ambient rock of multi-orifice nozzle hydrothermal jet [1]. Besides, Song et al. proposed and compared two kinds of cooling configurations (Lateral configuration and downward configuration) for a single hydrothermal jet drilling [2]. However, only water was considered in the previous study, while the reaction products contain both water and carbon dioxide.

In this paper, three materials, including compressible water, carbon dioxide and cuttings are considered and the downhole flow field of the lateral cooling configuration is investigated. **Figure 2** illustrates the details of the cooling configuration where the red region represents thermal fluid and blue region represents cooling water. Transient flow field is analyzed to approximate the steady state. Influences of the jet temperature, cooling water velocity, carbon dioxide volume fraction and type of rock on the flow field are discussed. Results in this paper can be more similar to the real situation during the drilling process.

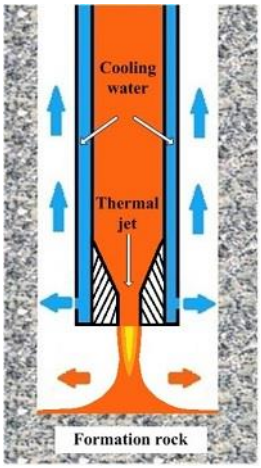

Figure 2. Lateral cooling configuration

2 MODEL SETUP

2.1 Physical model

To simplify the numerical simulation of this axisymmetric circular drilling model, a two-dimensional model is used to represent the real three-dimensional situation as shown in **Figure 3**. According to the cooling configurations described above, the hydrothermal jet, including water and carbon dioxide, is discharged from the central nozzle, while the cooling water flows out from the lateral outlets. The drill cuttings are cumulated at the well bottom. To ensure the results could reflect the distribution regularities of the hydrothermal jet in the entire wellbore, the length of the wellbore is set at 300 mm. The borehole diameter is set at 50.8 mm. The coiled tubing diameter is 25.4 mm. The jet nozzle diameter and the cooling water inlet are 10 mm. Mesh is generated by Gambit using structural grids. Because the analyzed region is very short compared to the thousands of meters of well depth, friction loss between the fluid and wellbore is neglected. **Figure 3** shows the mesh when the standoff distance is 30mm and mesh interval size is 1.

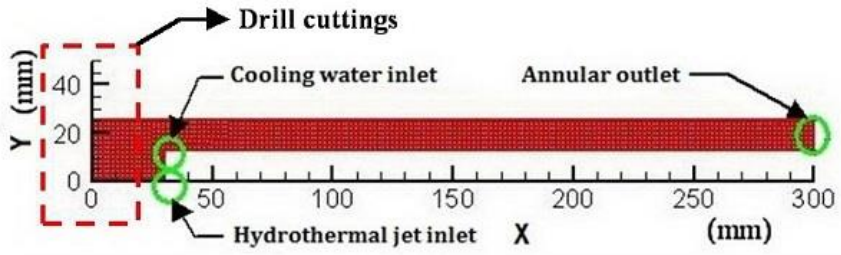

Figure 3. Mesh of the model of standoff distance 30mm

Recognizing the process of hydrothermal jet drilling, the boundary conditions are set as follows: velocity inlet boundary conditions are set for the hydrothermal jet and cooling water inlets. Outflow boundary condition: all the injected fluid flows out from the annulus. Stationary wall boundary condition: in the process of numerical simulation, the wellbore and the drilling pipe are stationary. Besides, the operating pressure is set as 30 MPa to model the environment at the depth approximately 3000 m in the reservoir.

2.2 Thermo-physical properties of supercritical water

When the high-temperature hydrothermal jet encounters with the peripheral cooling water, drastic heat and momentum transfer occur. The simulation of supercritical water with varying thermo-physical properties is rather complicated [7, 8]. Four characteristics of water, including density, specific heat capacity, viscosity and thermal conductivity, are the most important factors in the calculation of the jet process. In this paper, the varying trends of water density and specific heat capacity are shown in **Figure 4** at the pressure of 30 MPa [9, 10].

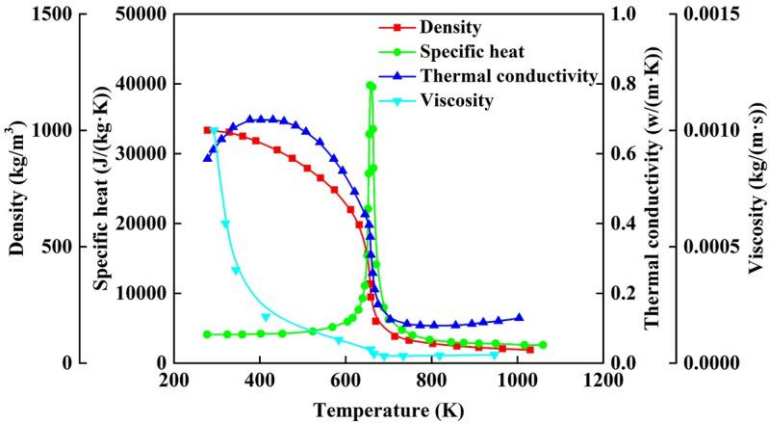

Figure 4. Thermo-physical properties of water at the pressure of 30 MPa

The water density decreases as the rise of temperature, which can be as low as 100 kg/m^3. However, the specific heat capacity changes in a wide range. For each supercritical pressure, there is a corresponding temperature yielding the maximum value of specific heat capacity at the so-called pseudo-critical point (PCP). This temperature is called the pseudo-critical temperature (PCT). The line connecting all these pseudo-critical points is named pseudo-critical line (PCL). In the vicinity of this PCL, all thermo-physical properties are very sensitive to temperature variations by undergoing sharp changes. In order to simulate the process of water thermo-physical property change more accurately, the least square method with piecewise-polynomial equations is adopted to simulate the varying of water property change.

2.3 Equation of state for carbon dioxide

The Peng-Robinson equation of state is applied in the simulation of property change for carbon dioxide. Peng-Robinson is a model that is commonly used both in industry and academia as it is relatively accurate for the prediction of vapor pressure, density and other thermo-dynamic properties of non-polar and slightly polar fluids [11]. Because the molecule of carbon dioxide tends to be non-polar, the Peng-Robinson equation of state may be sufficient for the modeling.

The general form of pressure P for the cubic equation of state model is written as:

$$P = \frac{RT}{V - b + c} - \frac{\alpha}{(V^2 + \delta V + \varepsilon)} \tag{1}$$

Where P represents the absolute pressure, Pa. V represents the specific molar volume,

m^3/kmol. T is the temperature, K. R is the universal gas constant. In addition, the coefficients α, b, c, δ and ε are given for each equation of state as functions of the critical temperature T_c, critical pressure P_c, acentric factor ω and critical volume V_c. The attractive coefficient α also has a temperature dependence.

$$\alpha(T) = \alpha_0[1 + n(1 - (T / T_c)^{0.5}]^2 \tag{2}$$

$$\alpha_0 = \frac{0.457247 R^2 T_c^2}{P_c} \tag{3}$$

$$b = \frac{0.07780 R T_c}{P_c} \tag{4}$$

$$n = 0.37464 + 1.54226\omega - 0.26992\omega^2 \tag{5}$$

Besides, δ is set equal to $2b$. ε is equal to $-b^2$ and c is set to zero.

2.4 Modeling method

To keep the water jet in critical state, the jet temperature is initially set at 673 K. The hydrothermal jet velocity is set at 100 m/s according to the general velocity of the high pressure water jet. The cooling water temperature is set at temperature (293 K) which is easy to obtain for practical use. Gravity (9.81 m/s^2) is considered in the model. The fuel (methane) and oxidizer (oxygen) are injected to the downhole combustion chamber through separate conduits.

$$CH_4 + 2O_2 \rightarrow CO_2 + 2H_2O$$

The stoichiometric relationship between carbon dioxide and water is 1:2. Therefore, the volume fraction of carbon dioxide in the generated hydrothermal jet is initially set as 30%. The drill cuttings are initial set at the well bottom with a height of 20 mm. The granite is considered with a density of 2650 kg/m^3. The shape of the drill cutting is neglected. The temperature of the drill cutting is set at 333 K, which is the reservoir temperature at the depth of approximately 2 km. The schiller-naumann is applied to simulate the interaction between the drill cuttings and fluid. Turbulent flow calculation is carried out by using Realizable $k-\varepsilon$ model, which is widely used at present [7, 8, 12]. The Eulerian model, viscous heating and equations energy model solved by FLUENT are also chosen. The semi-implicit method for pressure-linked (SIMPLE) algorithm with multi-grid solver is used to couple pressure and velocities. Under-relaxation factors are set as default values. The convergence criterion based on residuals is set as 1×10^{-4} for each equation. The initial interval size of the mesh is 0.6. Other grids are checked for grid independence and produce similar results.

3 RESULTS AND DISCUSSION

3.1 Transient downhole flow field

Since the drill cuttings are initially set at the well bottom, the total amount of the drill cuttings

is fixed. The transient downhole flow field of carbon dioxide volume fraction is shown in **Figure 5**. The hydrothermal jet is discharged from the nozzle, impinges the bottom rock and returns through the annulus. There are two vortexes in the bottomhole space with the maximum carbon dioxide volume fraction. At 0.002 s, the hydrothermal jet reaches the well bottom. Then at 0.003 s, the jet fluid occupies the well bottom. After that, the fluid begins to return to the surface through the annulus. The volume fraction of carbon dioxide is 10% in most of the downhole space.

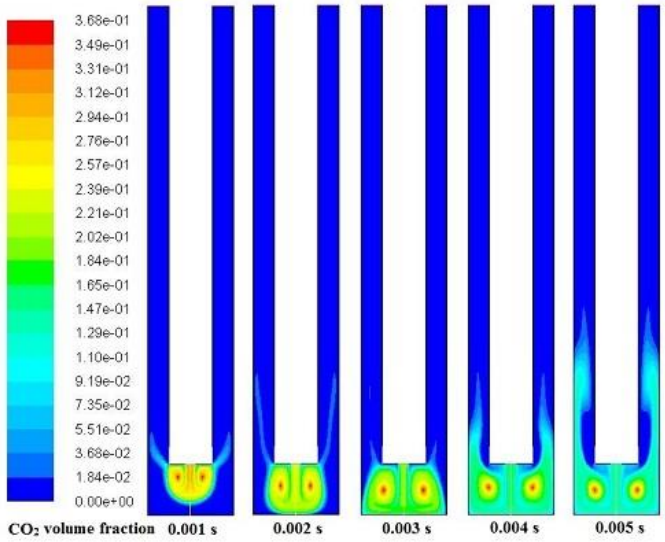

Figure 5. Contours of carbon dioxide volume fraction in the downhole flow field

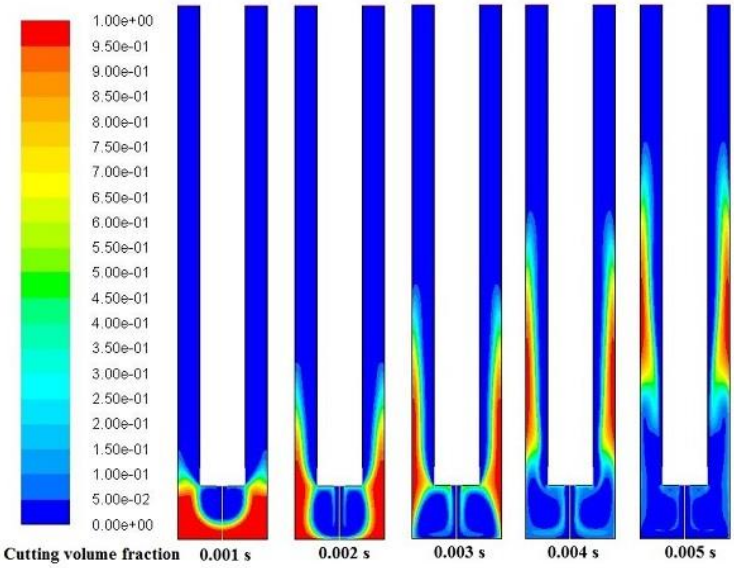

Figure 6. Contours of cutting volume fraction in the downhole flow field

To analyze the effect of hydrothermal jet on the bottom cuttings, **Figure 6** shows the distributions of drill cuttings at different times. At 0.001 s, the hydrothermal jet pushes the cuttings to the annulus. At 0.002 s, the cuttings are uniformly distributed around the wellbore. Then the hydrothermal fluid carries the cuttings to the surface through the annulus. Therefore, the transient process of carrying a certain amount of cuttings from the bottomhole can be simulated. However, it is not an easy task to model the steady rock breaking state that the cuttings can be generated constantly from the well bottom. In this paper, a transient state is

assumed to represent the steady state. Here, the flow field at 0.002 s is adopted because at this moment, the hydrothermal jet approximately reaches the well bottom to break the bottom rock and the cuttings are carried out around the wellbore. The downhole situation at this state is very similar to the constant drilling process.

3.2 Effects of jet temperature

Figure 7 shows the contours of cutting volume fraction at different jet temperatures. In fact, the jet temperature can have an effect on the thermo-physical properties of the hydrothermal jet. It can be observed that when the jet temperature is 673 K, the well bottom cuttings are cleaned out. However, for jet temperatures of 773 K, 873 K and 973 K, there is still a small thickness of cuttings distributed at the well bottom. The cutting-cleaning effect may not be better with increasing jet temperature. It may be better to keep the jet temperature close to the PCT.

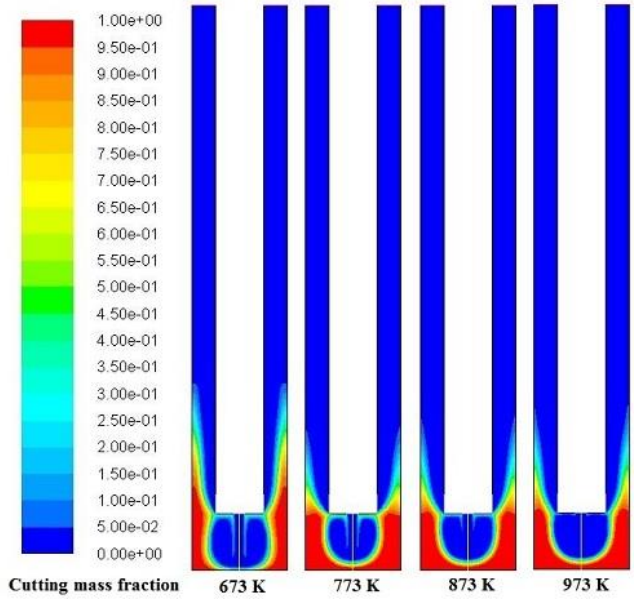

Figure 7. Contours of cutting mass fraction at different jet temperatures

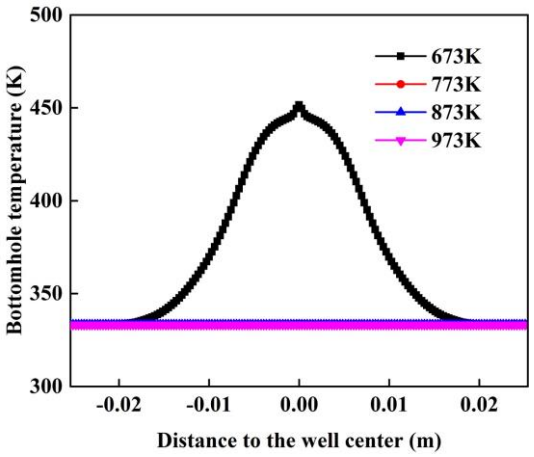

Figure 8. Distributions of bottomhole pressure at different jet temperatures

Correspondingly, in **Figure 9**, only the hydrothermal jet with a temperature of 673 K reaches the well bottom. The temperature at the well bottom center is the highest, while the

temperature at the periphery of the bottom is initial rock temperature. With respect to the bottomhole pressure, the centerline pressure is the highest. Here, the density of the hydrothermal jet decreases as the rise of temperature. Therefore, less impact force is generated as the increase of temperature.

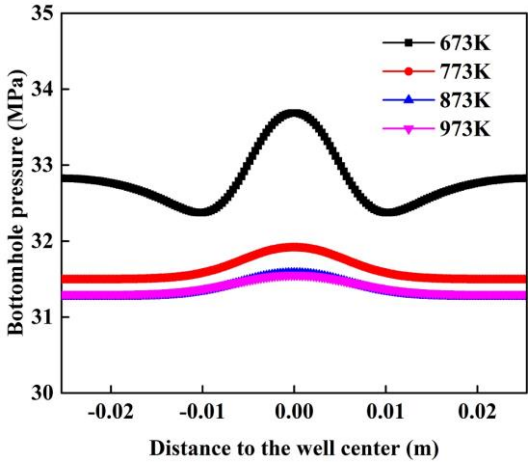

Figure 9. Distributions of bottomhole pressure at different jet temperatures

3.3 Effects of cooling water velocity

In hydrothermal jet drilling, the cooling water is injected to cool the bottomhole assembly and wellbore preventing the occurrence of collapse. **Figure 10** shows the distributions of cutting volume fraction at different cooling water velocities. It can be observed that the distributions of cuttings are similar at different cooling water velocities. Although the inlet direction of cooling water is perpendicular to the return direction of hydrothermal fluid, the increase of cooling water velocity has no obvious effect on the carrying of drill cuttings. With respect to the bottomhole temperature, as shown in **Figure 11**, the temperature at the well bottom center becomes slightly higher as the increase of cooling water velocity.

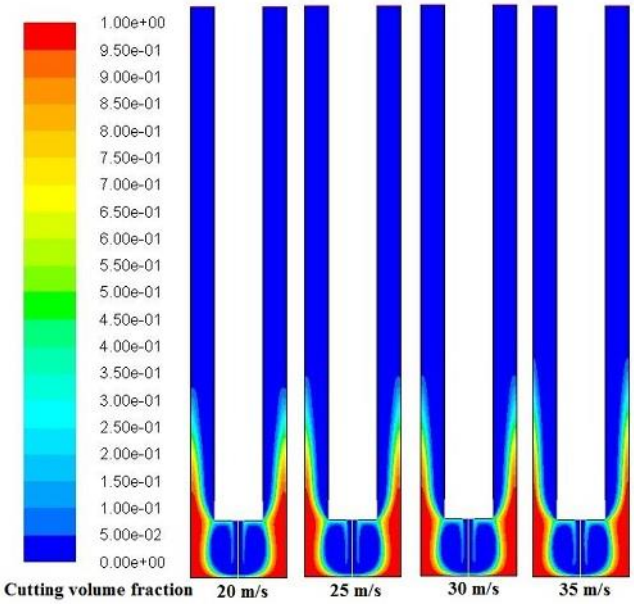

Figure 10. Distributions of cutting volume fraction at different cooling water velocities

Similarly, as shown in **Figure 12**, the bottomhole pressure also increases. This is because the inlet of hydrothermal jet set in this paper is constant velocity boundary condition. When the cooling water velocity increases, it becomes difficult for bottom space hydrothermal fluid to return from the annulus. Therefore, to keep the inlet velocity constant, the inlet pressure has to be increased. Thus, the bottomhole temperature and pressure can be improved.

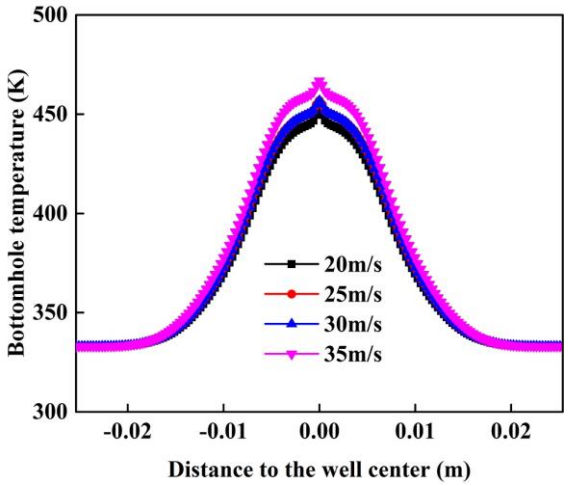

Figure 11. Distributions of bottomhole pressure at different cooling water velocities

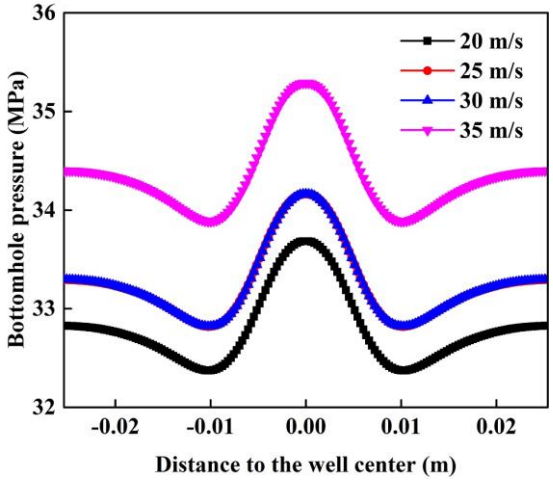

Figure 12. Distributions of bottomhole pressure at different cooling water velocities

3.4 Effects of carbon dioxide volume fraction

The above simulation of water and carbon dioxide volume fraction are based on the stoichiometric relationship. In hydrothermal jet drilling, additional water can be injected to the reactor to enhance the generation of hydrothermal jet. Consequently, the water volume fraction can be increased or carbon dioxide fraction can be decreased in the final generated jet.

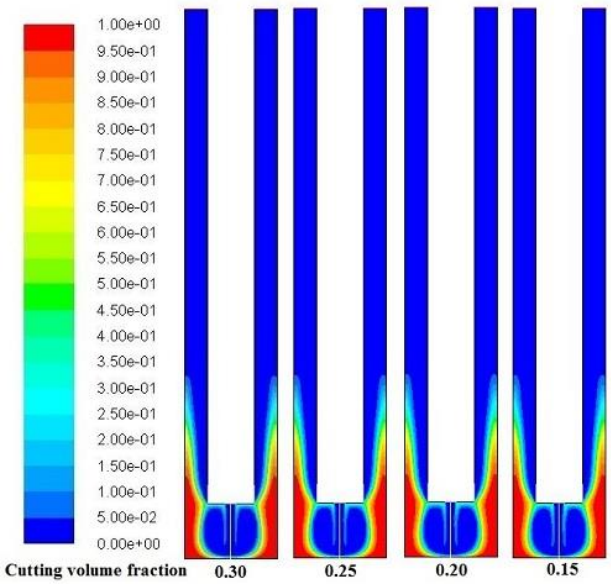

Figure 13. Distributions of cuttings at different carbon dioxide volume fractions

Figure 13 shows the distributions of cuttings at different carbon dioxide volume fractions. The decrease of carbon dioxide volume fraction can be assumed to be the increase of water fraction. It can be observed that the increase of water amount has no influence on the distributions of drill cuttings. With respect to the bottomhole temperature and pressure, they both rise as the increase of water volume fraction as shown in **Figure 14** and **Figure 15**. Under the condition of constant jet velocity, the final pressure impinging on the bottom rock is most related to the jet density. The addition of the water volume fraction changes the components or density of the hydrothermal jet. In supercritical state, the density of water may be slightly higher than that of carbon dioxide, which gives higher impact force. The higher impact force makes the hydrothermal jet much easier to clean the bottom drill cuttings to obtain higher bottomhole temperature.

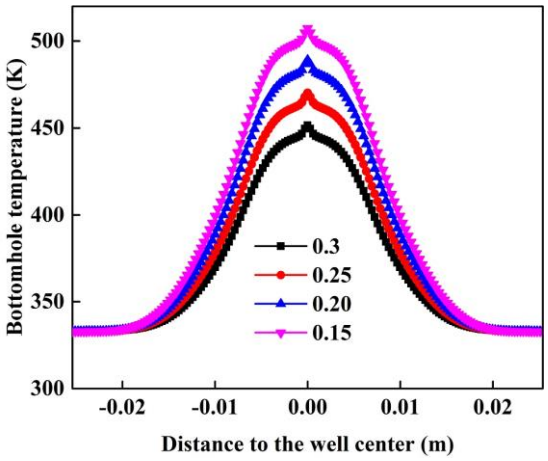

Figure 14. Distributions of bottomhole temperature at different carbon dioxide volume fractions

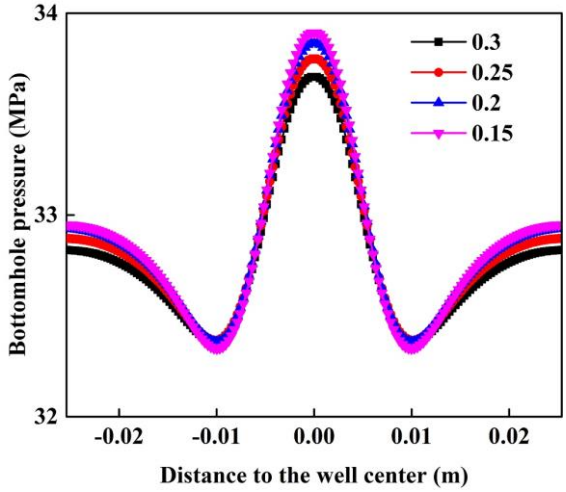

Figure 15. Distributions of bottomhole pressure at different carbon dioxide volume fractions

3.5 Effects of rock type

Different types of rock may be encountered during hydrothermal jet drilling. In this paper, four types of rock, including sandstone, granite, limestone and dolomite, are selected. Since the thermal interaction between the fluid and cuttings is neglected, only density is considered for different rocks as shown in **Table 1**. The density increases from sandstone to dolomite.

Table 1. Densities of different types of rock

Rock type	Density, kg/m^3
Sandstone	2180
Granite	2650
Limestone	2720
Dolomite	2840

As shown in **Figure 16**, there are no obvious differences of downhole distributions of cuttings of different types of rock. However, with respect to the bottomhole temperature as shown in **Figure 17**, the temperature of sandstone is the highest. Also, the maximum temperature decreases as the increase of rock density. This may because it is clean efficiency is higher for cuttings with low density. Then the high temperature jet is more likely to reach the well bottom. In addition, the range of high temperature decreases as the increase of rock density. The low temperature cuttings can be pushed away more easily for cuttings with low density.

With respect to the bottomhole pressure as shown in **Figure 18**, the pressures at the well bottom center are the same for different types of rock because the pressure at this stagnation point is only related to the hydrothermal jet. However, at parts around the well bottom center (approximate 0.01 m to the center), the pressure rises as the increase of rock density. Since the absolute pressure is used in this paper, the low value of pressure means that the velocity in this position is high. Therefore, for sandstone, the radial velocity at the well bottom is the highest, which means that it is easier to clean the cuttings of sandstone.

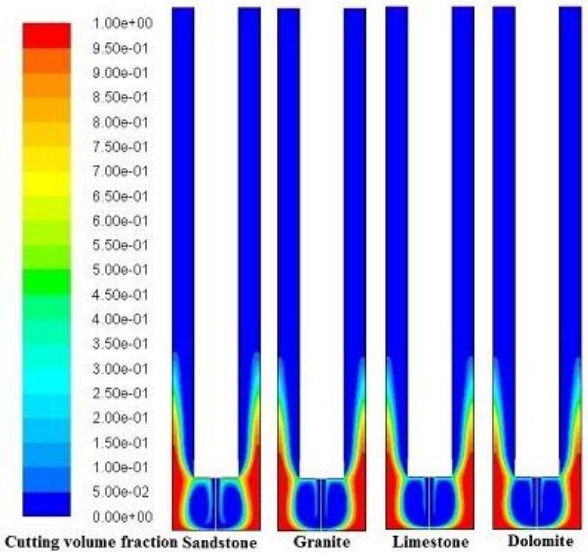

Figure 16. Contours of cutting volume fraction of different rock types

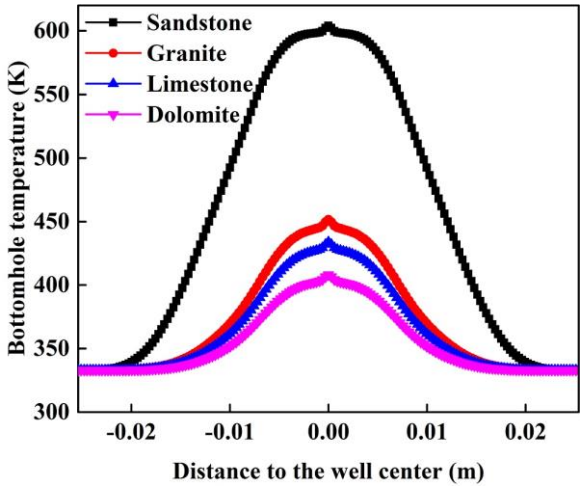

Figure 17. Distributions of bottomhole temperature of different rock types

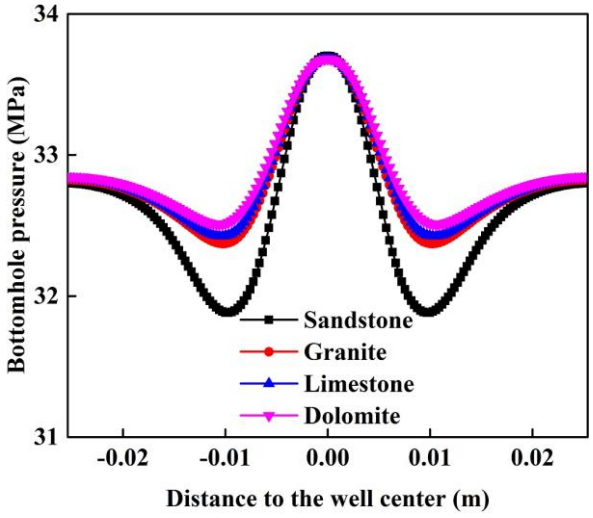

Figure 18. Distributions of bottomhole pressure of different rock types

4 CONCLUSIONS

With respect to the downhole flow field, there are two vortexes in the bottomhole space with the maximum carbon dioxide volume fraction. At 0.002 s, the hydrothermal jet reaches the well bottom. Then at 0.003 s, the jet fluid occupies the well bottom. After that, the fluid begins to return to the surface through the annulus. The volume fraction of carbon dioxide is 10% in most of the downhole space.

During the drilling process, it may be better to keep the jet temperature close to the PCT. The increase of cooling water velocity has no obvious effect on the carrying of drill cuttings. In supercritical state, the density of water may be slightly higher than that of carbon dioxide, which gives higher impact force. The higher impact force makes the hydrothermal jet much easier to clean the bottom drill cuttings to obtain higher bottomhole temperature.

The maximum temperature decreases as the increase of rock density. This may because it is clean efficiency is higher for cuttings with low density. Then the high temperature jet is more likely to reach the well bottom. In addition, the range of high temperature decreases as the increase of rock density. The low temperature cuttings can be pushed away more easily for cuttings with low density. The clean efficiency for low density rocks is higher.

ACKNOWLEDGMENTS

The authors would like to acknowledge the National Key Research and Development Program of China (2016YFE0124600), Program of Introducing Talents of Discipline to Chinese Universities (111 Plan) (B17045) and National Natural Science Foundation of China (51504272, U1562212, 51521063). Besides, support from Special Fund of Ministry of Education for Authors of Outstanding Doctoral Dissertations (201352) and China National Petroleum Corporation Innovation Fund (2015D-5006-0308) and New Technique and Method Fund (2016A-3902) are appreciated.

REFERENCES

[1] X. Song, Z. Lv, G. Li, et al. Numerical analysis of characteristics of multi-orifice nozzle hydrothermal jet impact flow field and heat transfer, Journal of Natural Gas Science and Engineering, 2016, 35, 79-88.

[2] X. Song, Z. Lv, G. Li, et al. Numerical analysis on the impact of the flow field of hydrothermal jet drilling for geothermal wells in a confined cooling environment. Geothermics, 2017, 39–49.

[3] Heard, H., 1980. Thermal expansion and inferred permeability of climax quartz monzonite to 300℃ and 27.6MPa. Int J Rock Mech Min Sci&GeomechAbstr. 1980, 289-296.

[4] Li, J., Guo, B., Yang, S., Liu, G., 2014. The complexity of thermal effect on rock failure in gas-drilling shale-gas wells. Journal of Natural Gas Science and Engineering. 2014, 255-259.

[5] Maurer, W.C, Heilhecker, J.K, 1969. Hydraulic Jet Drilling. Paper of the Drilling and Rock Mechanics Symposium.

[6] Pols, A.C., 1977. High-pressure jet-drilling experiments in some hard rocks. J. Press. Vessel Technol. 99 (2), 353-361.

[7] Martin, J., Tobias, R., Philipp, R., Simulation of the thermal field of submerged supercritical water jets at near-critical pressures. The Journal of Supercritical Fluids. 2013, 128-137.

[8] Martin J., Tobias R., Philipp, R., Numerical analysis of penetration lengths in submerged supercritical water jets. The Journal of Supercritical Fluids. 2013, 82, 213-220.

[9] Wagner W. The IAPWS Formulation 1995 for the Thermodynamic Properties of Ordinary Water Substance for General and Scientific Use. Journal of Physical & Chemical Reference Data, 2002, 31(2), 387-535.
[10] Peng, Y., Ma, C., 2005. Technical Application Manual of Supercritical Fluid. 2005, 417-437.
[11] D. Peng, D.B. Robinson, A New Two-Constant Equation of State, 15 (1976), 59–64.
[12] Tobias R. et al., Heat transfer phenomena of supercritical water jets in hydrothermal spallation drilling. 2013.